Diamond & Related Materials 163 (2026) 113437

Contents lists available at ScienceDirect

Diamond & Related Materials

journal homepage: www.elsevier.com/locate/diamond

NIR-emission of fluorine-related color centers in diamond

S. Ditalia Tchernij [a,b,e], M. Ziino [a,b], E. Corte [a,b], G. Gavello [a], C. Verona [c], T. Lühmann [d], G. Verona-Rinati [c], G. Petrini [a,e], F. Picariello [a], I.P. Degiovanni [e,b], S. Pezzagna [d], M. Genovese [e,b], J. Meijer [d], P. Olivero [a,b,e], J. Forneris [a,b,e,*]

[a] Physics Department, University of Torino, 10125, Turin, Italy
[b] Istituto Nazionale Di Fisica Nucleare (INFN), Sezione Di Torino, 10125, Turin, Italy
[c] INFN–Dipartimento di Ingegneria Industriale, Università di Roma "Tor Vergata", Roma, Italy
[d] Applied Quantum Systems, Felix-Bloch Institute for Solid-State Physics, Universität Leipzig, 04103, Leipzig, Germany
[e] Istituto Nazionale Di Ricerca Metrologica (INRiM), 10135, Turin, Italy

ARTICLE INFO

Keywords:
NIR emission
Fluorine color centers
Diamond defects
Photoluminescence
Cathodoluminescence
Electroluminescence
Quantum emitters

ABSTRACT

This study explores luminescence emission characteristics of fluorine-related color centers in diamond fabricated by ion implantation and subsequent thermal annealing. Photoluminescence, cathodoluminescence, and electroluminescence analysis were performed, revealing distinct emission features in the near-infrared region. In particular, a novel emission line identified at 990 nm is consistent with theoretical predictions for the optical activity of the negatively charged substitutional fluorine color center.

1. Introduction

The pursuit of robust solid-state quantum emitters operating under ambient conditions has established diamond color centers as appealing candidates for quantum optics and information processing [1]. While the Nitrogen-Vacancy (NV) center remains the most extensively studied defect [2,3], significant research efforts are dedicated to identifying and characterizing new quantum emitters with optimal opto-physical properties, particularly those with zero-phonon lines (ZPLs) within the near-infrared (NIR) or telecommunications range [4–7]. Among them, integrating halogen impurities, such as Fluorine, into the diamond lattice represents a promising avenue for engineering novel spin-active defects [8,9]. A preliminary high-throughput experimental work on emitters screening in diamond identified F ion implantation followed by thermal annealing as an effective method to create optically active color centers in high-purity diamond [4]. Further systematic characterization confirmed that the photoluminescence (PL) in F-ion-implanted diamond can be attributed to a stable defective complex incorporating the above-mentioned impurity in the diamond lattice [10]. The room-temperature PL spectrum displays a broad emission band in the 600–800 nm spectral range. Cooling the samples to liquid Helium temperature resolves this visible emission into a more structured set of characteristic lines in the 600–670 nm spectral range (F-center), with the overall intensity correlating directly with the F ion implantation fluence [10]. Concurrently, theoretical investigations were conducted to address the nature and the potential for technological applications of halogen-related defects in diamond. While early models explored the stability of impurity-vacancy complexes [9], a recent work has focused on the fluorine substitutional defect in the negative charge state (F_C^{-1}). First-principles calculations predicted that the F_C^{-1} defect is structurally stable and is characterized by a triplet ground state with optically addressable transitions [8]. Remarkably, the emission energy of the Zero Phonon Line (ZPL) of the F_C^{-1} center was theoretically predicted to be 1.26 eV (984 nm): if confirmed, this would represent an appealing feature, since it belongs to the near-infrared range [8]. In this work, we experimentally address the prediction of a NIR emission from the F_C^{-1} center in diamond by searching for new luminescence lines in the near-infrared region. We utilize multiple excitation regimes, namely photoluminescence (PL), cathodoluminescence (CL), and electroluminescence (EL), to explore the optical transitions of the F-related defects. We discuss the excitability under these different excitation regimes to provide a deeper understanding of the F-related color center in diamond.

* Corresponding author at: Physics Department, University of Torino, 10125, Turin, Italy.
E-mail address: jacopo.forneris@unito.it (J. Forneris).

https://doi.org/10.1016/j.diamond.2026.113437
Received 28 November 2025; Received in revised form 28 January 2026; Accepted 10 February 2026
Available online 11 February 2026

2. Experimental

2.1. Sample preparation

This study was conducted on two artificial diamond samples produced by ElementSix via Chemical Vapor Deposition (CVD) synthesis. The first sample (*Sample A*) is a 2 × 2 × 0.5 mm^3 electronic-grade diamond, which was selected for its low impurity levels, with nominal concentrations of both substitutional nitrogen (N) and boron (B) below 5 ppb. This high purity was essential to ensure that the subsequent PL analysis would isolate the spectral features of the F_C^1 center by minimizing background emission from other intrinsic defects. The second substrate (*Sample B*) is an optical-grade diamond (3 × 3 × 0.3 mm^3) containing higher impurity concentrations ($N < 1$ ppm, B < 0.05 ppm). This sample was employed for CL experiments, aiming at the discrimination of the spectral features of the F_C center against those of the well-known Nitrogen-Vacancy (NV) center, which is natively abundant in this grade of diamond.

Both samples were implanted with 50 keV F^- ions using a low-energy accelerator through a circular beam collimator (~175 μm diameter) placed at ~5 mm distance from their surface. This enabled to implant different regions having the same nominal area as the collimated beam. Ion implantation was performed at fluences of 5 × 10^{15} cm^{-2} and 1 × 10^{13} cm^{-2} on Samples A and B, respectively. Following the ion implantation, both samples underwent a two-stage thermal and chemical treatment: firstly, a high-temperature thermal annealing was performed (1200 °C for 4 h under high vacuum at ~10^{-6} mbar). This processing step yields different results depending on the degree of amorphization caused by the implantation: if the diamond is damaged past the graphitization threshold, the material is converted into graphite, whereas if the material has suffered a smaller amount of damage, the diamond lattice is mostly recovered as vacancies diffuse and interstitials anneal, promoting the formation of stable F-related color centers. After thermal annealing, an oxygen plasma treatment (60 Pa pressure, 0.5 sccm O2 flux, 30 min duration, 23 W microwave power) was applied to suppress any spurious background fluorescence caused by residual surface contaminants.

It is worth noting that the ion implantation fluence adopted for *Sample A* resulted in a vacancy density exceeding the graphitization threshold for a significant portion of the longitudinal F^- ions range. Fig. 1a (black line) shows a simulation of the vacancy density profile performed according to SRIM Monte Carlo code in "full damage cascade" mode, setting a 50 eV displacement energy for the diamond lattice [11,12]. This profile was obtained by multiplying the single ion vacancy linear density profile with the ion fluence, thus not taking into account saturation effects (e.g. defect-defect interaction, self-annealing, etc.) at damage densities approaching the material amorphization threshold. From a comparison with the graphitization threshold, estimated as 6 × 10^{22} cm^{-3} for implanted ions in the keV range [13] and shown in Fig. 1a as the blue horizontal line, it is apparent that the entire implanted volume down to a depth of 70 nm was converted into a graphitic phase upon the adopted post-implantation thermal annealing. The subsequent plasma cleaning etched the graphite, uncovering the implanted material the end of range of the F^- ions (Fig. 1b). The longitudinal ions distribution, simulated by SRIM code and shown in red in Fig. 1a. indicates that a residual concentration of the implanted F ions (quantified in ~15%) stopped at larger depths (70–100 nm) and was thus still present in the material following the removal of the graphitized layer, where it had taken part in the formation of optically active F-related centers.

Furthermore, the spacing between the ion collimator and the sample surface resulted in the implantation of scattered ions at the edge of the collimation mask. This resulted in the formation of an "irradiation halo" area [14] characterized by an effective ion fluence that is lower than the nominal one achieved at the center of the designed implantation area (Fig. 1b). As a result, a buried graphitized layer was formed on an annular region surrounding the implantation area, which was not affected by the post-implantation treatments (Fig. 1b–c). This conductive layer, after being directly exposed to the surface of the diamond sample by the removal of the circular graphitized region, was electrically contacted to external circuitry via metallic indium. A graphite-diamond-metal junction was then fabricated by depositing 200 nm Ag to form a second electrode with a ~ 10 μm spacing from the graphitic ring (sketch in Fig. 1c). The Ag electrode was in turn connected to external circuitry with a metallic indium electrical contact. Finally, it is worth remarking that F impurities were implanted in a wider annular

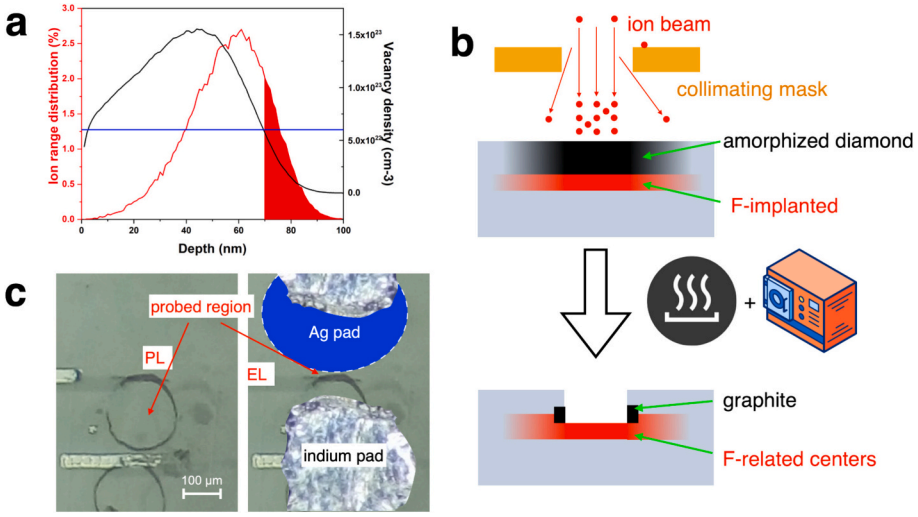

Fig. 1. a) SRIM simulation of 50 keV F^- ion implantation in diamond: vacancy density profile for 5 × 10^{15} cm^{-2} ion fluence (black line), graphitization threshold for keV-implanted diamond (blue line), longitudinal ion range distribution (red line). The area filled in red highlights the fraction of ions implanted below the diamond layer experiencing graphitization at the considered ion fluence. b) Schematic representation of the region processed on *Sample A*. The ion implantation through a collimation mask results in the graphitization of a surface layer according to panel a. The ion-mask scattering causes ion implantation at the outer edge of the implanted region, with ion fluence decreasing at increasing scattering angles. The thermal annealing and the oxygen plasma treatment cause the graphitization and subsequent removal of the upper layer of the implanted region. c) optical micrograph of *Sample A*. The red arrows indicate the F-implanted regions probed under PL/CL spectroscopy and EL analysis, respectively. The black arrow points to the residual annular graphitic region at the edge of the implanted area. The fabrication of electrical contacts is also sketched. (For interpretation of the references to color in this figure legend, the reader is referred to the web version of this article.)

region surrounding the graphitic circle visible in (Fig. 1c), with a fluence decreasing with the distance from the designed implantation area (Fig. 1c).

2.2. PL and EL analysis

PL characterization was performed using a custom confocal microscope (100×, 0.90 NA dry objective, ~350 nm Airy disk radius at focus) equipped with single-photon sensitive avalanche detectors (SPAD) [10] and driven by open source Qudi software [15]. Optical excitation was provided by a 520 nm CW laser decoupled from the collection path via a 550 nm long pass dichroic mirror and further filtered out by an additional 550 nm long pass optical filter. Additional spectral analysis at higher excitation wavelengths was performed using a 80 MHz pulsed tunable laser source (NKT Fianum 15) in combination with a 750 nm cutoff dichroic mirror and long pass filters. The PL spectra were acquired by feeding the fiber coupled output of the confocal microscope to a Single Photon Avalanche Detector (SPAD) by Excelitas (<200 cps dark noise) via a motorized, computer-controlled monochromator (~4 nm spectral resolution [14]). The photon count rate was recorded as a function of the selected wavelength to acquire emission spectra of the sample from the center of the F-implanted region. EL analysis was performed adopting the same experimental setup. In this case, the optical excitation was replaced by the current injected in the active region of the junction, i.e. at the outer edge of the graphitic ring (see Fig. 1c).

2.3. CL analysis

CL analysis was performed at room temperature using a "Cambridge S260" scanning electron microscope (SEM) as the cathodoluminescence excitation source. The electron-beam energy was set to around 10 kV, corresponding to an emitting region located about 0.5 μm beneath the diamond surface [16]. Luminescence from the irradiated surface was collected with a paraboloidal mirror and directed, via a retractable light-collection system, onto the entrance slit of an "Applied Photophysics f/3.4" monochromator (1200 mm^{-1}, 300 nm blaze). The signal was detected with a Hamamatsu Photonics E717–21 photomultiplier tube. Spectra were acquired over the 550–1100 nm (~2,25–1.13 eV) range and were not corrected for the wavelength-dependent response of the optical system, whose sensitivity starts to decline at approximately 650 nm.

3. Results

A room-temperature PL spectrum acquired from the center of the processed region of *Sample A* (see Fig. 1c) is shown in the 550–1000 nm range in Fig. 2a under 520 nm laser excitation. The spectrum exhibits the typical features of the F-related center emission, namely a broad band in the 600–800 nm range, with the possible occurrence of a ZPL at 600 nm. These features, absent in a pristine region of the sample as extensively shown in a previous work [10], are fully in line with the occurrence of the F-related center [4,10]. Notably, no spectral emission was detected in the NIR range. The excitability of a F-related NIR emission was also investigated by considering longer laser wavelengths. Fig. 2b shows the PL spectra acquired in the 750–1000 nm range under 532 nm, 640 nm, 660 nm and 700 nm excitation wavelengths, for which no apparent luminescence signal was detected.

Conversely, Fig. 2c reports the CL spectra acquired from *Sample B*, where a comparison is shown between the optical signature of pristine material (red line) and that of the region implanted with F^- ions (black line). The unimplanted region clearly shows the CL spectrum of the neutrally charged Nitrogen-Vacancy center (NV^0) in diamond [17,18], denoted by a sharp ZPL at 575 nm followed by a phonon sideband in the 575–700 nm range. This feature is typical of CL and EL excitation, in which the photon emission is mediated by an electron-hole pair recombination mechanism. The poor efficiency of this process for the negatively charged Nitrogen-Vacancy center (NV^-) typically makes the emission of the latter center (i.e. 638 nm) undetectable [18]. On the other hand, the CL spectrum acquired from the F-implanted region of *Sample B* highlights the occurrence of additional PL features. This spectrum represents a composite profile, combining the original NV^0 emission spectrum and the spectrum of F-related center in Fig. 2a. This attribution is in line with the absence of new ZPL features in the 550–800 nm range, and by the increased PL intensity in the longer wavelength region (e.g., ~650–800 nm). Notably, the CL spectrum evidences an additional emission line at 990 nm, not visible in the pristine region of the material and previously unreported in the scientific literature in ion irradiated diamond, to the best of the authors knowledge. The emission line can be thus attributed to a F-containing defect, and it can be tentatively assigned to the ZPL of the F_C^{-1} center, given its close agreement with the predicted theoretical value of 984 nm [8]. The moderate intensity of this peak in the uncalibrated spectra in Fig. 2 is attributed to the detection efficiency of the detector, which is less than 5% at 1000 nm wavelength according to the manufacturer datasheet. Considering similar inefficiencies for the monochromator diffraction gratings and the other optical elements, the emission intensity is expected to be comparable with that of the F-related band at 600–800 nm..

The graphite-diamond-metal junction fabricated in *Sample A* was instrumental in assessing the spectral signatures of F-related centers in EL regime. Fig. 3a shows a PL confocal microscopy map (520 nm, 200 μW excitation laser) of the implanted region. A bright circular fluorescent area is visible, consistently with the geometry of the sample described in Fig. 1c. The bright region is located between two dark areas, consisting of the optically opaque metallic layers forming the junction. Similarly, the dark ring within the circular high-emitting region corresponds to the graphitized annular region at the edge of the implanted

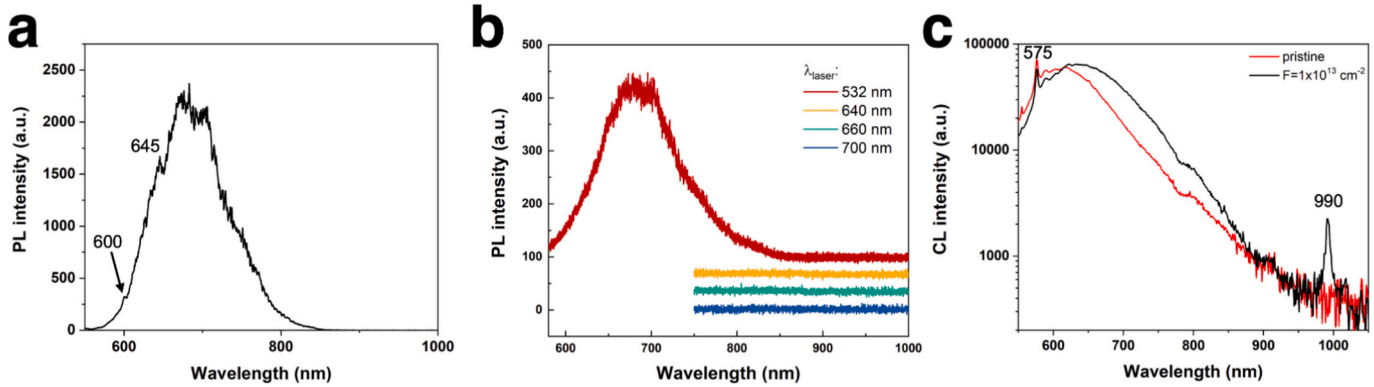

Fig. 2. a) Photoluminescence emission spectrum acquired from the F-implanted region of *Sample A*. b) Stacked PL spectra of the same region under pulsed laser excitation at 532 nm, 640 nm, 660 nm, 700 nm. c) Cathodoluminescence emission spectrum acquired from the F-implanted region of *Sample B*.

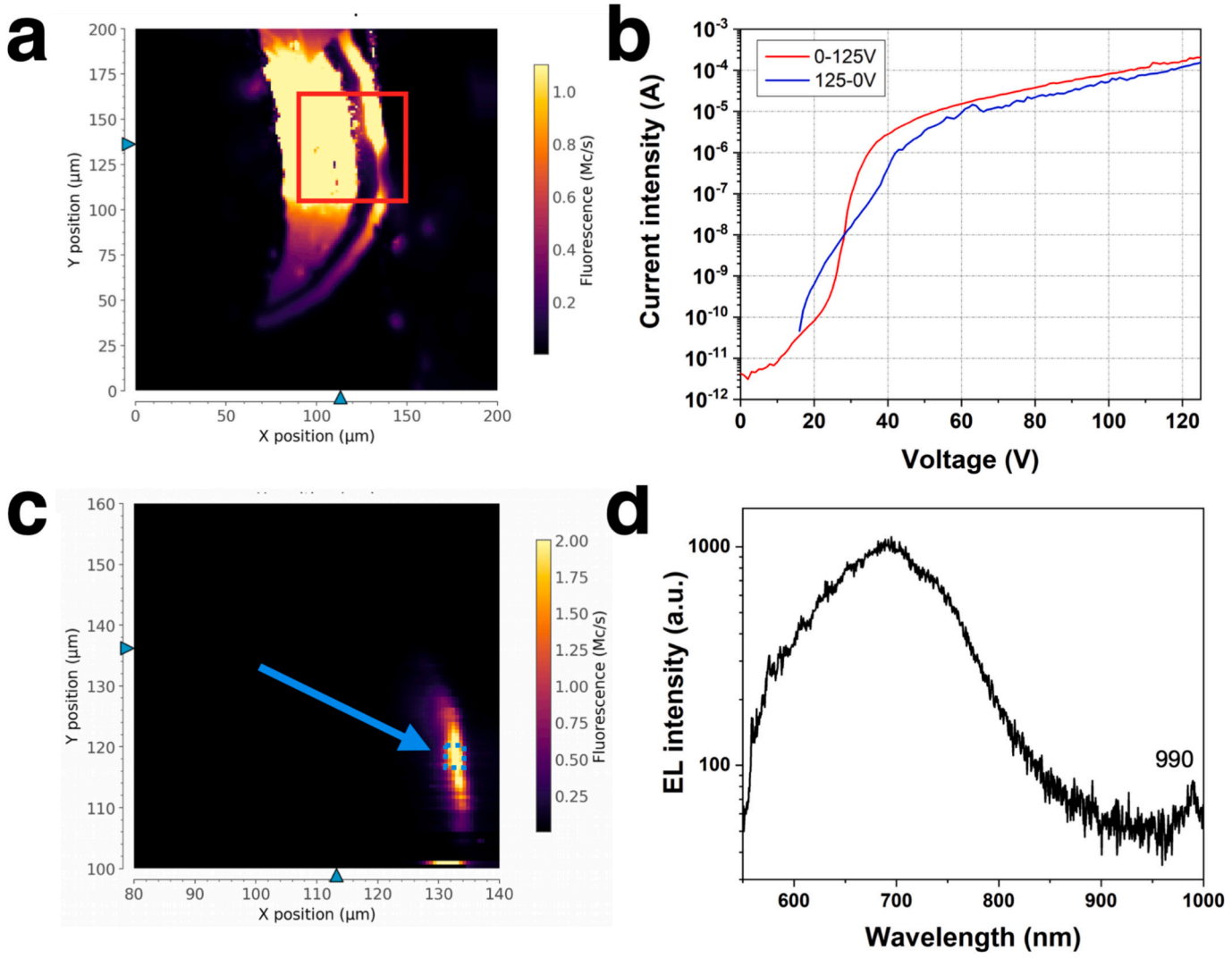

Fig. 3. a) Photoluminescence map (520 nm excitation, 550 nm long-pass filtering))of the F-implanted region in *Sample A*. b) Current-voltage characteristic of the graphite-diamond-metal junction fabricated at the outer edge of *Sample A*. c) Electroluminescence map (550 nm long-pass filtering) acquired from the region highlighted in red in panel a under constant 125 V voltage bias. d) Electroluminescence emission spectrum acquired from the bright spot highlighted by the blue square in panel c. (For interpretation of the references to color in this figure legend, the reader is referred to the web version of this article.)

area. EL analysis was preceded by an electrical characterization of the junction by means of current-voltage characteristics (Fig. 3b) in the 0–125 V bias range. Similarly to what observed in previous works on graphite-diamond-graphite junctions [19], the current exhibits an almost linear trend at low bias voltages (0–20 V, red curve), followed by a space-charge-limited-driven sudden variation, spanning over 5 orders of magnitude in the 20–40 V range, where currents up to tens of µA are recorded. At higher voltages, the current stabilizes to an exponential trend in the 40–125 V bias range, which was attributed to a Poole-Frenkel conduction mechanism [20]. The role of electron trapping at lattice defects in the electrical conduction is further corroborated by the pronounced current hysteresis observed when reverting the voltage back to zero (blue line in Fig. 3b). The EL emission was investigated by removing the optical excitation from the sample and holding the junction at a constant voltage of 125 V during the analysis. Fig. 3c shows a typical EL confocal microscopy map acquired from the region highlighted in red in Fig. 3a under the same conditions. The map clearly shows bright ensemble emission (>2 Mcps) from the portion of the sample between the graphitic electrode and the outer Ag electrical contact, indicating that the current flow is concentrated in the active region of the junction. An EL emission spectrum acquired under the above-mentioned experimental conditions is shown in Fig. 3d. The spectrum highlights the same optical signatures observed in Fig. 2, namely the F-related intense emission band in the 600–800 nm range. The lack of NV center emission is a consequence of the low concentration of native N impurities in *Sample A* and is consistent with the PL spectrum observed in Fig. 2a. Notably, the 990 nm emission peak observed in CL regime in Fig. 2c is also clearly visible, thus confirming the role of carrier recombination at F-related defects at the origin of this emission line.

4. Conclusions

In this work, we provide experimental evidence for NIR photon emission at 990 nm from F-related color centers in diamond. The emission was observed in cathodoluminescence and electroluminescence regimes but could not be achieved under optical excitation in the 520–700 nm range. This latter point, in contrast with the optical addressability predicted in Ref. [8], suggests that the emission process involves the recombination of electron-hole pairs, or that alternatively the involved energy levels are ionized upon photon absorption in the considered excitation wavelengths range due to their proximity to the semiconductor energy bands. The observed emission wavelength is still in striking agreement with the theoretical predictions made for the

substitutional F center in its negative charge state [8]. This evidence leads thus to the tentative assignment of the observed spectral line to the F_C^{-1} center.

The relation of the 990 nm emission with the previously reported F-related band at 600–800 nm is still unclear. On one hand, both the substitutional F [8] model and the F-vacancy [9] models propose a charge state transition at ~3 eV, which is compatible with the experimental measurements reported in Ref. [10] against different excitation wavelengths. Furthermore, in both cases the emission in the visible range would be assigned to the neutral charge state of either defect.

In perspective, the lack of optical excitability for the 990 nm F-related emission line can be overcome by the electrical control of the defect, which in principle could enable its integration in high-density optoelectronic devices. This electrical control would combine with the theoretically predicted appealing spin properties (triplet states with zero-field splitting in the GHz range [8]), with potential applications in quantum-enhanced sensing and information processing [21–24].

CRediT authorship contribution statement

S. Ditalia Tchernij: Writing – review & editing, Validation, Methodology, Investigation, Data curation. **M. Ziino:** Writing – review & editing, Validation, Investigation, Formal analysis. **E. Corte:** Visualization, Methodology, Investigation. **G. Gavello:** Visualization, Investigation, Formal analysis. **C. Verona:** Writing – review & editing, Methodology, Investigation, Formal analysis, Data curation. **T. Lühmann:** Writing – review & editing, Resources, Methodology, Investigation. **G. Verona-Rinati:** Writing – review & editing, Methodology, Investigation, Formal analysis, Data curation, Conceptualization. **G. Petrini:** Writing – review & editing, Methodology, Investigation, Formal analysis, Data curation. **F. Picariello:** Writing – review & editing, Validation, Methodology, Investigation. **I.P. Degiovanni:** Writing – review & editing, Resources, Methodology. **S. Pezzagna:** Writing – review & editing, Validation, Supervision, Resources. **M. Genovese:** Writing – review & editing, Supervision, Resources, Funding acquisition. **J. Meijer:** Writing – review & editing, Supervision, Resources, Methodology. **P. Olivero:** Writing – original draft, Supervision, Resources, Conceptualization. **J. Forneris:** Writing – review & editing, Writing – original draft, Visualization, Validation, Supervision, Resources, Methodology, Investigation, Funding acquisition, Formal analysis, Conceptualization.

Declaration of competing interest

The authors declare that they have no known competing financial interests or personal relationships that could have appeared to influence the work reported in this paper.

Acknowledgements

This work was supported by the following projects: Project “Piemonte Quantum Enabling Technologies” (PiQuET), funded by the Piemonte Region within the “Infra-P” scheme (POR-FESR 2014-2020 program of the European Union); the experiments QUISS funded by the 5th National Commission of the Italian National Institute for Nuclear Physics (INFN), Project PROMISE (this project has received funding from the European Union's Horizon Europe – The EU research & innovation programme under the Grant Agreement number 101189611). JF acknowledges financial support under the National Recovery and Resilience Plan (NRRP), Mission 4, Component 2, Investment 1.1, Call for tender No. 1409 published on 14.9.2022 by the Italian Ministry of University and Research (MUR), funded by the European Union–NextGenerationEU– Project P2022KSTSR- Opto-mechanical effects in spin-defects for quantum technologies- CUP D53D23019370001, and PNRR MUR project PE_00000023- SPOKE 4- CUP B53C22004170006. The project contributing to this work 23NRM04 NoQTeS has received funding from the European Partnership on Metrology, co-financed from the European Union's Horizon Europe Research and Innovation Programme and by the Participating States.

Data availability

Data will be made available on request.

References

[1] L.V.H. Rodgers, L.B. Hughes, M. Xie, P.C. Maurer, S. Kolkowitz, A.C. Bleszynski Jayich, N.P. de Leon, Materials challenges for quantum technologies based on color centers in diamond, MRS Bull. 46 (2021) 623.
[2] M.W. Doherty, N.B. Manson, P. Delaney, F. Jelezko, J. Wrachtrup, L.C. L. Hollenberg, The nitrogen-vacancy colour centre in diamond, Phys. Rep. 528 (2013) 1.
[3] R. Katsumi, K. Takada, F. Jelezko, T. Yatsui, Recent progress in hybrid diamond photonics for quantum information processing and sensing, Commun. Eng. 4 (2025) 85.
[4] T. Lühmann, N. Raatz, R. John, M. Lesik, J. Rödiger, M. Portail, D. Wildanger, F. Kleißler, K. Nordlund, A. Zaitsev, J.-F. Roch, A. Tallaire, J. Meijer, S. Pezzagna, et al., Screening and engineering of colour centres in diamond, J. Phys. D. Appl. Phys. 51 (2018) 483002.
[5] I. Aharonovich, C. Zhou, A. Stacey, J. Orwa, S. Castelletto, D. Simpson, A. D. Greentree, F. Treussart, J.-F. Roch, S. Prawer, Enhanced single-photon emission in the near infrared from a diamond color center, Phys. Rev. B 79 (2009) 235316.
[6] A.I. Shames, A. Dalis, A.D. Greentree, B.C. Gibson, H. Abe, T. Ohshima, O. Shenderova, A. Zaitsev, P. Reineck, Near-infrared fluorescence from silicon- and nickel-based color centers in high-pressure high-temperature diamond micro- and nanoparticles, Adv. Opt. Mater. 8 (2020) 2001047.
[7] S. Mukherjee, Z.-H. Zhang, D.G. Oblinsky, M.O. de Vries, B.C. Johnson, B. C. Gibson, E.L.H. Mayes, A.M. Edmonds, N. Palmer, M.L. Markham, Á. Gali, G. Thiering, A. Dalis, T. Dumm, G.D. Scholes, A. Stacey, P. Reineck, N.P. de Leon, A telecom O-band emitter in diamond, Nano Lett. 23 (2023) 2557.
[8] P.-P. Filippatos, A. Chroneos, N. Kelaidis, A first-principles investigation of halogen doped diamond and its application to quantum technologies, J. Appl. Phys. 138 (2025) 094401.
[9] J.P. Goss, P.R. Briddon, M.J. Rayson, S.J. Sque, R. Jones, Vacancy-impurity complexes and limitations for implantation doping of diamond, Phys. Rev. B 72 (2005) 035214.
[10] S. Ditalia Tchernij, T. Lühmann, E. Corte, F. Sardi, F. Picollo, P. Traina, M. Brajkovic, A. Crnjac, S. Pezzagna, Z. Pastuovic, I.P. Degiovanni, E. Moreva, P. Apra, P. Olivero, Z. Siketic, J. Meijer, M. Genovese, J. Forneris, Fluorine-based color centers in diamond, Sci. Rep. 10 (2020) 21537.
[11] J.F. Ziegler, M.D. Ziegler, J.O. Biersack, SRIM—the stopping and range of ions in mat- ter, Nucl. Instrum. Meth. B 268 (2010) 1818.
[12] D. Saada, J. Adler, R. Kalish, Transformation of diamond (sp^3) to graphite (sp^2) bonds by ion-impact, Int. J. Mod. Phys. C 9 (1998) 61.
[13] A. Britel, A. Kuriakose, E. Nieto Hernández, E. Corte, S. Ditalia Tchernij, P. Aprà, S. Sturari, N.-H. Amine, V. Pugliese, E. Redolfi, J. Forneris, P. Olivero, O. Jedrkiewicz, F. Picollo, Comparative analysis of diamond graphitization approaches for 3D electrode fabrication, J. Mater. Sci. Mater. Electron. 36 (2025) 1150.
[14] S. Ditalia Tchernij, T. Lühmann, T. Herzig, J. Küpper, A. Damin, S. Santonocito, M. Signorile, P. Traina, E. Moreva, F. Celegato, S. Pezzagna, I.P. Degiovanni, P. Olivero, M. Jakšić, J. Meijer, M. Genovese, J. Forneris, Single-photon emitters in lead-implanted single-crystal diamond, ACS Photonics 5 (2018) 4864.
[15] J.M. Binder, A. Stark, N. Tomek, J. Scheuer, F. Frank, K.D. Jahnke, C. Müller, S. Schmitt, M.H. Metsch, T. Unden, T. Gehring, A. Huck, U.L. Andersen, L. J. Rogers, F. Jelezko, Qudi: a modular python suite for experiment control and data processing, SoftwareX 6 (2017) 85.
[16] G. Davies, in: J.E. Field (Ed.), The Properties of Diamond, Academic, London, 1979.
[17] A.M. Zaitsev, Optical Properties of Diamond, Springer, New York, 2001.
[18] J. Chen, C. Shinei, J. Inoue, H. Abe, T. Ohshima, T. Sekiguchi, T. Teraji, Appearance of spectral dip in the cathodoluminescence spectrum of negatively charged nitrogen-vacancy centers in diamonds, Diam. Relat. Mater. 148 (2024) 111476.
[19] S. Ditalia Tchernij, N. Skukan, F. Picollo, A. Battiato, V. Grilj, G. Amato, L. Boarino, E. Enrico, M. Jakšić, P. Olivero, J. Forneris, Electrical characterization of a graphite-diamond-graphite junction fabricated by MeV carbon implantation, Diam. Relat. Mater. 74 (2017) 125.
[20] J. Forneris, S. Ditalia Tchernij, A. Tengattini, E. Enrico, V. Grilj, N. Skukan, G. Amato, L. Boarino, M. Jakšić, P. Olivero, Electrical control of deep NV centers in diamond by means of sub-superficial graphitic micro-electrodes, Carbon 113 (2017) 76.
[21] A.M. Day, M. Sutula, J.R. Dietz, A. Raun, D.D. Sukachev, M.K. Bhaskar, E.L. Hu, Electrical manipulation of telecom color centers in silicon, Nat. Commun. 15 (2024) 4722.
[22] P. Siyushev, M. Nesladek, E. Bourgeois, M. Gulka, J. Hruby, T. Yamamoto, M. Trupke, T. Teraji, J. Isoya, F. Jelezko, Photoelectrical imaging and coherent

spin-state readout of single nitrogen-vacancy centers in diamond, Science 363 (2019) 728.
[23] P.V. Klimov, A.L. Falk, B.B. Buckley, D.D. Awschalom, Electrically driven spin resonance in silicon carbide color centers, Phys. Rev. Lett. 112 (2014) 087601.
[24] G. Petrini, E. Moreva, E. Bernardi, P. Traina, G. Tomagra, V. Carabelli, I. P. Degiovanni, M. Genovese, Is a quantum biosensing revolution approaching? Perspectives in NV-assisted current and thermal biosensing in living cells, Adv. Quantum Technol. 2 (2020) 2000066.